A&A manuscript no.
(will be inserted by hand later)

Your thesaurus codes are:
11.17.1;11.17.4 APM08279+5255

ASTRONOMY AND ASTROPHYSICS

Structure of the Mg II and damped Lyman-α systems along the line of sight to APM 08279+5255 ⋆

Patrick Petitjean[1,2], Bastien Aracil[1], R. Srianand[3], and Rodrigo Ibata[4]

[1]Institut d'Astrophysique de Paris – CNRS, 98bis Boulevard Arago, F-75014 Paris, France
[2]UA CNRS 173 – DAEC, Observatoire de Paris-Meudon, F-92195 Meudon Cedex, France
[3]IUCAA, Post Bag 4, Ganesh Khind, Pune 411 007, India
[4]Max-Plank Institut für Astronomie, Königstuhl 17, D-69117 Heidelberg, Germany

Abstract. A study of the absorption systems toward the gravitationally lensed quasar APM 08279+5255 is presented.

Most of the Mg II systems in the redshift range $z \sim 1.2$–2.07, although saturated, show large residuals at the bottom of the lines. The most likely interpretation is that individual clouds within Mg II halos do cover only one of the two brightest QSO images. The separation between the two lines of sight decreases from 1.7 to 0.7 h_{75}^{-1} kpc ($q_o = 0.5$, $z_{lens} = 1$) between $z = 1.22$ and $z = 2.07$. This reveals that Mg II halos are made of a collection of clouds of radius smaller than about 1 h_{75}^{-1} kpc.

Two strong Mg II absorbers at $z_{abs} = 1.062$ and 1.181 are studied in detail. This is the first time that the Na Iλ3303 doublet is detected in such high redshift systems. Together with the detection of the Mg Iλ2852 transition, this strongly constrains the physical characteristics of the gas. The N(Na I)/N(Mg I) ratio is found to be larger than unity, implying that the gas is cool and neutral. The Doppler parameters measured in individual and well detached components is probably as small as 1 km s^{-1}. The column densities of Na I, Ca II, Mg I, Ti II, Mn II and Fe II observed at $z_{abs} = 1.1801$ are very close to that observed along the line of sight towards 23 Ori in our Galaxy. The shape of the QSO continuum is consistent with attenuation by dust at $z \sim 1$ ($A_V \sim 0.5$ mag). Altogether it is found that the H I column density at $z = 1$ is of the order of 1 to 5 10^{21} cm^{-2}, the corresponding metallicity is in the range 1–0.3 $Z_\odot$, the overall dust-to-metal ratio is about half that in our Galaxy and the relative depletion of iron, titanium, manganese and calcium is similar to what is observed in cool gas in the disk of our Galaxy. The objects associated with these two systems could both contribute to the lens together with another possible strong system at $z_{abs} = 1.1727$ and the strong Lyman-α system at $z_{abs} = 2.974$.

The probable damped Lyman-α system at $z_{abs} = 2.974$ has $19.8 < \log N(\text{H I}) < 20.3$. The transverse dimension of the absorber is larger than 200 h_{75}^{-1} pc. Column densities of Al II, Fe II, Si II, C II and O I indicate abundances relative to solar of −2.31, −2.26, −2.10, −2.35 and −2.37 for, respectively, Fe, Al, Si, C and O (for $\log N(\text{H I}) = 20.3$). These surprizingly similar values indicate that the amount of dust in the cloud is very small as are any deviations from relative solar abundances. It seems likely that the upper limits found for the zinc metallicity of several damped Lyman-α systems at $z > 3$ in previous surveys is indicative of a true cosmological evolution of the metallicity in individual systems.

Key words: quasars: absorption lines, quasars: individual: APM 08279+5255

1. Introduction

The gravitationally lensed Broad Absorption Line (BAL) QSO APM 08279+5255 ($z_{em} = 3.911$) has been given much attention since its discovery by Irwin et al. (1998), as it is one of the most luminous objects in the universe even after correction for the gravitational lensing induced amplification. Adaptive-optics imaging has revealed two main components (Ledoux et al. 1998b), separated by 0.378±0.001 arcsec as measured on HST/NICMOS data (Ibata et al. 1999), and of relative brightness $F_B/F_A = 0.773 \pm 0.007$. The HST images reveal also the presence of a third object C with $F_C/F_A = 0.175 \pm 0.008$, located in between A and B and almost aligned with them. The point-spread-function model fits on the three objects are consistent with the three components being point-sources, and their colors are similar within the uncertainties. There is no trace of the lensing object up to magnitude $V = 23$.

Send offprint requests to: Patrick Petitjean

⋆ Based on observations collected at the W.M. Keck Observatory, which is operated as a scientific partnership among the California Institute of Technology, the University of California and the National Aeronautics and Space Administration. The Observatory was made possible by the generous financial support of the W.M. Keck Foundation.

A high S/N ratio high-resolution spectrum of APM 08279+5255 was obtained at the Keck telescope (Ellison et al. 1999a,b), and made available to the astronomical community. This spectrum, though complicated by the combination of light traveling along three different sightlines, is a unique laboratory for studying the intervening and associated absorption systems.

In this paper we study the structure of six intervening Mg II systems at $1.2 < z < 2.07$ and the physical characteristics of the gas in two very strong Mg II systems detected at $z_{\rm abs} = 1.06$ and 1.18, which, we argue, are damped Lyman-α systems and may well reveal the lensing galaxies. We also comment on a third probable damped Lyman-α system at $z_{\rm abs} = 2.974$. This paper is organized as follows: the data are described in Section 2; the structure of the intervening Mg II systems is investigated using the covering factor analysis in Section 3; we demonstrate that the Mg II systems at $z_{\rm abs} = 1.06$ and 1.18 are damped Lyman-α systems in Section 4; we discuss a probable damped Lyman-α system at $z_{\rm abs} = 2.974$ in Section 5. We adopt $H_{\rm o} = 75$ km s^{-1} Mpc^{-1} and $q_{\rm o} = 0.5$ througout the paper.

2. Data

A high S/N ratio, high-resolution spectrum of the $z_{\rm em} = 3.911$ quasar APM 08279+5255 was obtained with the HIRES echelle spectrograph at the 10m Keck-I telescope (Ellison et al. 1999a,b). This data was made public together with a low-resolution spectrum of the quasar and a high-resolution spectrum of a standard star. We have corrected the high-resolution spectrum of APM 08279+5255 for small discontinuities in the continuum, which are probably due to the inappropriate merging of different orders. These discontinuities have been recognized by comparing the high and low-resolution spectra. The latter is also used for normalization of the high-resolution data. Atmospheric absorption features were identified from the standard star spectrum. Voigt profile fitting of the absorption features have been performed using the context FITLYMAN (Fontana & Ballester 1995) of the European Southern Observatory data reduction package MIDAS and the code VPFIT (Carswell et al. 1987). We have measured the final spectral resolution by fitting the narrow atmospheric absorption lines which are free of blending. We find $FWHM \sim 8$ km s^{-1} ($b \sim 4.8$ km s^{-1}) at 6900 Å, $R = 37500$, and use this value throughout the paper.

3. Structure of the intervening $z > 1$ Mg II absorbers

Ellison et al. (1999b) have already noted that the two lines of some of the Mg II$\lambda\lambda$2796,2803 doublets cannot be fitted with the same column density and Doppler parameter. As can be seen on Fig. 1, most of the systems have a doublet

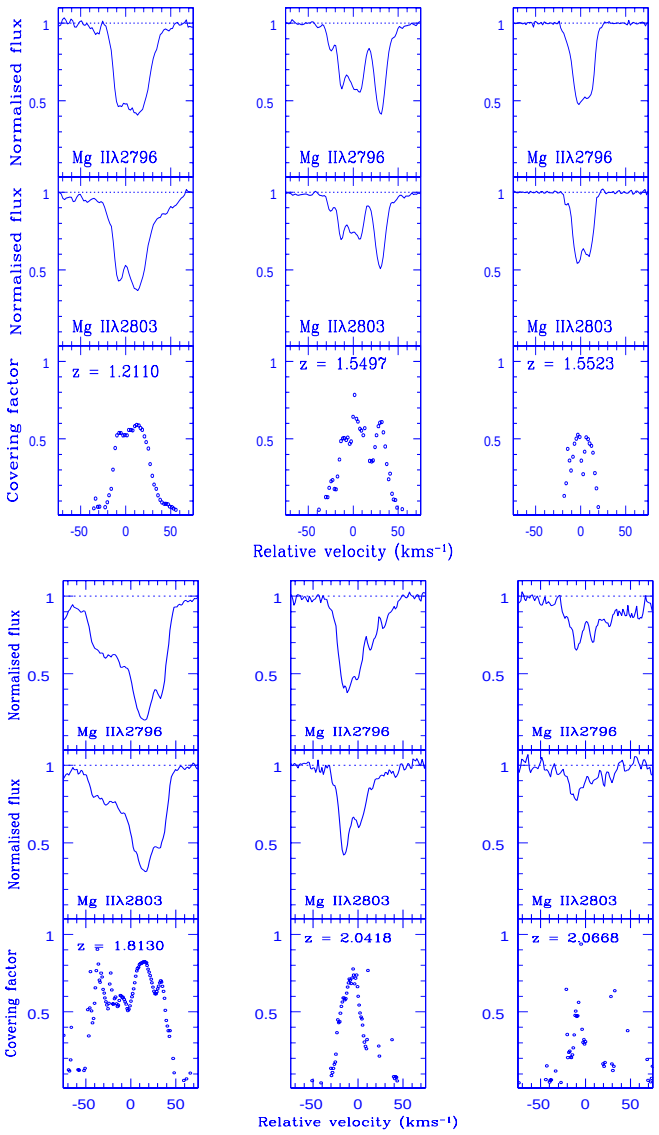

Fig. 1. Covering factor (bottom panels) of six Mg II systems observed along the line of sight to APM 08279+5255 calculated from the profiles of the Mg IIλ2796 (top panels) and Mg IIλ2803 (middle panels) absorptions.

ratio close to unity inspite of having residual intensities in the normalized spectrum close to 0.5.

If the background source is a point source and if the Mg IIλ2796 absorption line is resolved, then the residual intensity of the normalized spectrum measured at any velocity v with respect to the centroid of the line, is equal to $e^{-\tau(v)}$, where $\tau(v)$ is the optical depth at v and the residual intensity of the Mg IIλ2803 line is $e^{-\tau(v)/2}$. It is apparent from Fig. 1 that the above condition is not fullfilled for most of the Mg II doublets.

There are two possibilities to explain this. If the lines are not resolved, the measured residual intensity is affected by convolution of the true absorption profile

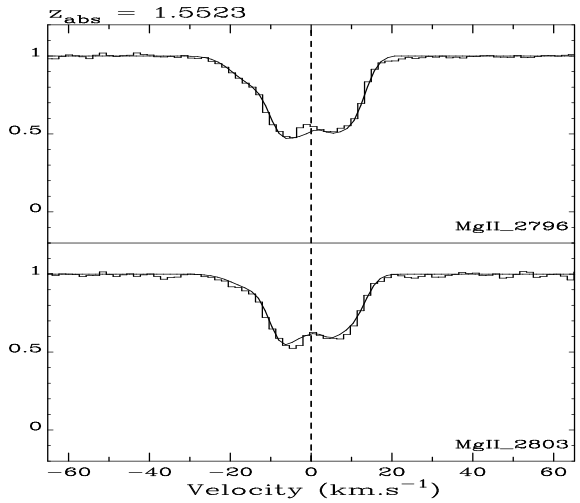

Fig. 2. Best fit of the Mg II doublet at $z_{\rm abs} = 1.5523$ with five narrow components ($b < 1.5$ km s^{-1}) and a covering factor $f = 1$ (reduced χ^2 of 1.5).

with the instrumental profile. This can introduce artificial residuals at the bottom of the saturated absorption features (see e.g. Lespine & Petitjean 1997). Alternatively, as the observed light is a combination of light from different images, it is possible that the column densities are different along different lines of sight and, as a limiting case, that the absorbing cloud does not cover all the images. We discuss these different possibilities below.

3.1. Unresolved narrow-components

If the absorption profiles are made up of unresolved components, the observed residual intensity does not correspond to the real optical depth. Given the resolution of the spectrum ($R \sim 37500$), a saturated Mg IIλ2796 line can have a residual intensity in the normalized spectrum of 0.5 if its Doppler parameter is smaller than 1.5 km s^{-1}. In that case, the residual intensity of the Mg IIλ2803 line is in the range 0.5–0.6, depending on the actual column density. The two equivalent widths differ by no more than 20% (see e.g. Lespine & Petitjean 1997).

The system at $z_{\rm abs} = 1.5497$ can be indeed fitted this way using 10 components with b values in the range 1.1–1.7 km s^{-1}. In that case the well detached cloud in the red wing (see Fig. 1) is fitted with two adhoc nearly identical components though the Mg IIλ2796 profile is perfectly fitted with a single *resolved* component model. However the one-component model cannot explain the strengths of the two Mg II lines without invoking partial coverage (see below).

We use the $z_{\rm abs} = 1.5523$ system to illustrate the case. The final spectrum has a defect in the center of the Mg IIλ2796 line. We have therefore used three individual exposures of high S/N ratio (Ellison private communication) to correct for this. The final optical depth variations from one spectrum to the other is about 2%. Fig. 2 shows the best fit to the doublet considering full coverage ($f = 1$). Five narrow components ($b < 1.5$ km s^{-1}) are needed. Although good (reduced χ^2 of 1.5), the fit is not completely satisfactory. We have fitted consistently the Mg II together with the Fe II lines considering that only one of the brightest sources is covered. With five components, a good fit (reduced χ^2 of 0.9), shown on Fig. 3, is obtained if B is not covered ($f = 0.6$). Details of the subcomponent parameters are given in Table 1. As the Mg II doublet ratio is close to one, small b values are needed even with the assumption of partial coverage.

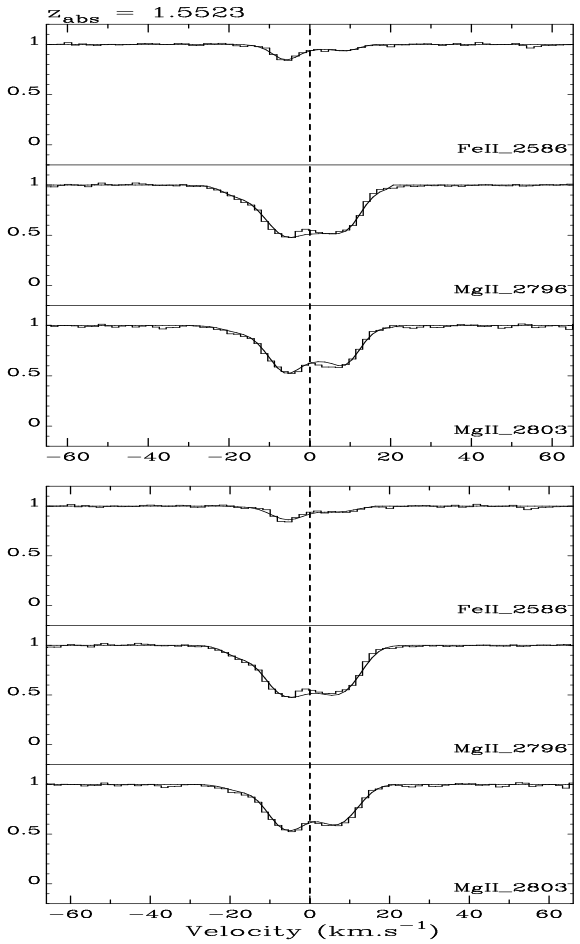

Fig. 3. Best fits of the $z_{\rm abs} = 1.5523$ Mg II and Fe II absorption lines obtained with five narrow ($b < 1.5$ km s^{-1}) components and $f = 0.6$ (*top panel*, reduced χ^2 of 0.9) and three broader ($b > 2.5$ km s^{-1}) components and $f = 0.45$ (*bottom panel*, reduced χ^2 of 0.6). The fit parameters are given in Table 1.

It should be noted however that a Doppler parameter smaller than 1.5 km s^{-1} corresponds to a temperature smaller than 3500 K, a surprizingly small temperature for this gas which is most probably ionized. Allowing for a smaller number of components, we can find a good fit with only three components, $f = 0.45$ and reduced $\chi^2 = 0.6$

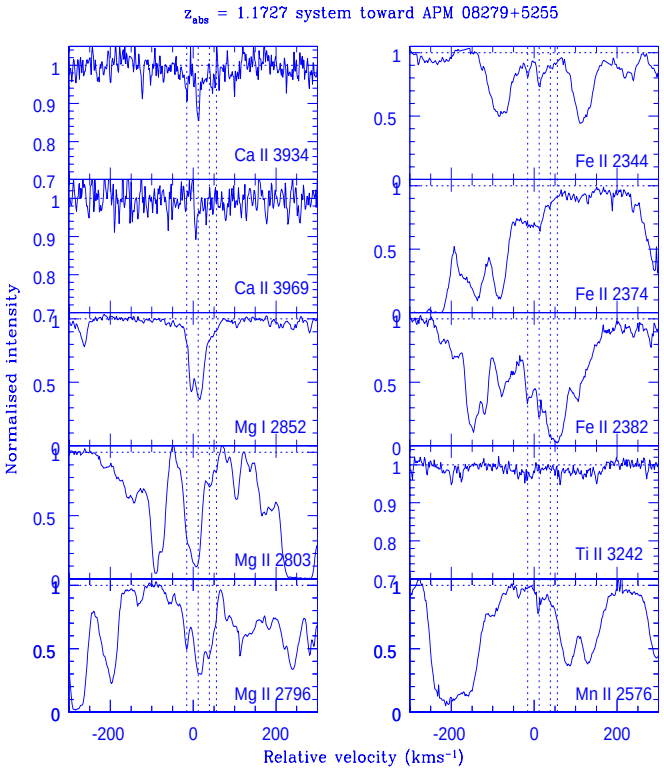

Fig. 4. Probable Mg II system at $z_{\rm abs} = 1.1727$. Most of the lines are blended but the similarity of the Fe II, Mg II and Ca II profiles supports the identification. Vertical dotted lines indicate the positions of the four probable components.

(see Fig. 3 and Table 1). The b values are larger than 2.5 km s^{-1} relaxing the restriction on the temperature.

A statistically acceptable fit is difficult to find for the systems at $z_{\rm abs} = 1.221$ and 1.5523. The red wing of the Mg IIλ2803 line at $z_{\rm abs} = 1.221$ is blended with another absorption feature which we found difficult to identify. It could be Mg Iλ2852 at $z_{\rm abs} = 1.1727$. This system is possibly detected by Fe II$\lambda\lambda$2344,2382, Mn IIλ2576 and Ca IIλ3934 (see Fig. 4). The other lines are either below the detection limit or blended. Confirmation of the Ca II lines, which are free of blending, would be particularly important as, probably, the presence of this additional system, together with the presence of the three damped systems at $z_{\rm abs} = 1.062$, 1.181 and 2.974 (see below) should be taken into account in any model of the lens.

3.2. Partial covering factor

3.2.1. Computing a covering factor

We can interpret the observations in terms of a covering factor which is the fraction of the background source covered by the absorbing cloud. The relative brightness of the three sources are $F_{\rm A,B,C}/F_{\rm tot} = 0.513$, 0.397 and 0.090 (Ibata et al. 1999). If one line-of-sight is completely absorbed (condition imposed by the fact that the doublets are saturated) and the other free of absorption, then the covering factor is 0.40, 0.49, 0.51 and 0.60 if, respectively, B only, B+C, A only and A+C are covered (the case C only is very unlikely as C is close to A and located in between A and B, Ibata et al. 1999; see however Srianand & Petitjean 2000). Given the uncertainties, if only one line-of-sight is completely absorbed, the covering factor should be in the range 0.4–0.6. Of course, it is larger if the second line-of-sight is not completely clear. We have computed the covering factor for the Mg II systems using the method described by Srianand & Shankaranarayanan (1999). This assumes that the lines are resolved. It can be seen in Fig. 1 that for the three systems with $z_{\rm abs} < 1.7$, the covering factor ranges between 0.5 and 0.6 whereas for the systems with $z > 1.7$, the covering factor is larger (but always less than 0.8) with the possible exception of the $z_{\rm abs} = 2.0668$ system. The latter system is quite weak however and uncertainties are large. The values of the covering factor for the three lower redshift systems suggest that the clouds cover one of the two brightest background sources only. This has to be investigated in more detail however.

Table 1. Fit parameters for the $z_{\rm abs} = 1.5523$ system

z	b^b	$\pm$	N(MgII)^a	$\pm$	N(FeII)^a	$\pm$
Best fit with five components; $f = 0.6$						
1.552165	1.7	0.5	11.51	0.15		
1.552219	1.1	0.5	11.88	0.05	11.67	0.12
1.552270	1.3	0.2	14.47	0.27	12.79	0.05
1.552338	3.4	0.2	12.47	0.10	12.23	0.06
1.552399	0.8	0.1	14.67	0.09	12.34	0.07
Best fit with three components; $f = 0.45$						
1.552170	2.9	0.5	11.67	0.10	11.29	0.11
1.552274	4.2	0.6	13.02	0.18	12.82	0.09
1.552378	4.6	0.7	12.85	0.20	12.44	0.07

^{a} logarithm of the column density in cm^{-2}
^{b} in km s^{-1}

3.2.2. Optical depths along different sightlines

In this Section we investigate the effect of the optical depth being different along different sight lines. In order to make our analysis simpler, we consider only two images, A and B, with fractional flux contributions $F_1 = 0.6$ and $F_2 = 0.4$. Suppose the optical depth along the two sight lines are τ_1 and τ_2 then the measured residual intensities are,

$$\begin{aligned} R(2796) &= F_1 e^{-\tau_1} + F_2 e^{-\tau_2} \\ R(2803) &= F_1 e^{-\tau_1/2} + F_2 e^{-\tau_2/2} \end{aligned} \quad (1)$$

The residual intensities can be written as (Srianand & Shankaranarayanan 1999),

$$R(2796) = 1 - f + f e^{-\tau} \quad (2)$$

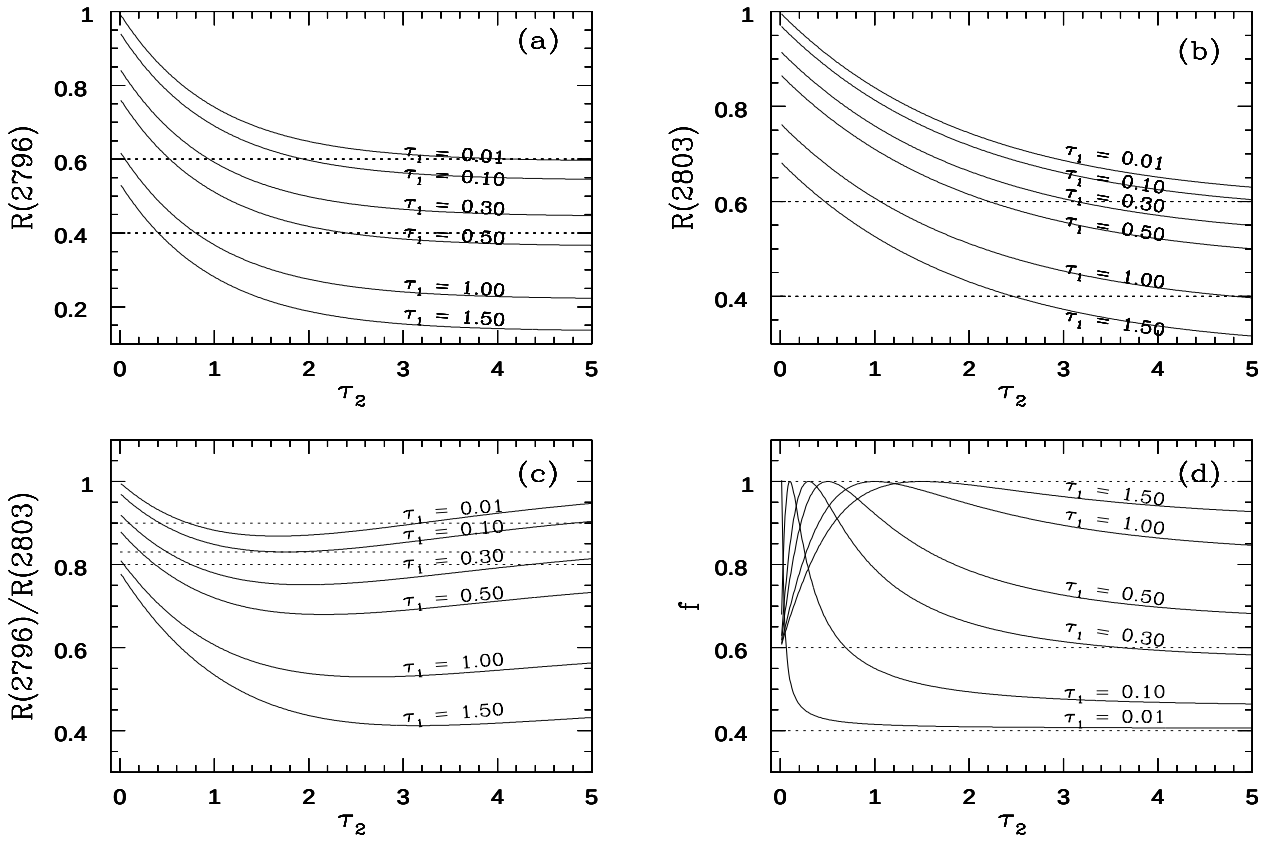

Fig. 5. Panels (a) and (b) give, respectively, the observed residuals $R(2796)$ and $R(2803)$ in the normalized spectrum and in the center of the Mg II$\lambda\lambda$2796,2803 lines as a function of τ_2 for different values of τ_1. τ_1 and τ_2 are the optical depths in the center of the Mg IIλ2796 line along, respectively, line of sight number one towards image A and line of sight number two towards image B (see Eqs. 1 and 2). It is assumed that the fractional flux contributions are $f_1 = 0.6$ and $f_2 = 0.4$. The two horizontal dotted lines show the range of observed values. Panel (c) gives the ratio of the residual intensities of the two absorption lines as a function of τ_2 for different values of τ_1. The dotted lines show the observed values in the three systems at $z_{\rm abs}< 1.7$. In panel (d) the derived covering factor f (Eq. 3) is shown as a function of τ_1 for different values of τ_2. Measured values are indicated by dotted horizontal lines.

$$R(2803) \;=\; 1 - f + fe^{-\tau/2}$$

where, f and τ are the resulting covering factor and optical depth and therefore,

$$f \;=\; \frac{[1 - R(2803)]^2}{1 + R(2796) - 2R(2803)} \qquad (3)$$

From Eqs. (1) and (3) one can derive f as a function of F_1, F_2, τ_1 and τ_2. This analysis assumes that the absorption profiles are resolved in the HIRES spectrum. As F_1 and F_2 are known from observation, the covering factor depends on τ_1 and τ_2 only.

In order to investigate the parameter space we have computed and plotted on Fig 5, the covering factor (panel d), residual intensities of the lines (panels a and b) and their ratio (panel c) as a function of τ_2 for different values of τ_1. In panels (a) and (b), the two horizontal dotted lines show the range of observed values for the Mg II systems with $z_{\rm abs}$<1.7. In panel (c) the dotted lines give the measured values for the three low-redshift Mg II systems.

As expected, when $\tau_1 = \tau_2$, $f = 1$ (albeit with various ratios of residual intensities) and for $\tau_1 \neq \tau_2$ the covering factors are less than 1.0. When $\tau_1 \geq \tau_2$ (respectively $\tau_1 \leq \tau_2$), the covering factor is in the range 0.6–1.0 (respectively 0.4–1.0). Conversely, the observed residual intensities, $R(2796)$ and $R(2803)$, together with the measured covering factor, f, can be used to constrain τ_1 and τ_2.

The covering factor estimates for $z_{\rm abs}< 1.7$ systems are in the range 0.5 and 0.6 (see Fig. 1). This, together with the observed residual intensities, indicates that the absorbing gas is saturated along one sight line only with optical depth ratios as large as ten. For example, the well detached component in the red wing of the $z_{\rm abs} = 1.5497$

system has $f = 0.6$ (with a typical error of 0.02), a residual intensity ratio ∼0.84 (with a typical error of 0.02) and R(2796)≃0.40 at the core of the line. This implies that the contribution to this absorption comes mainly from the line of sight toward A+C with the optical depth along B being more than an order of magnitude smaller.

3.3. Equivalent width ratio

The precise determination of the strength of the absorption lines along different lines of sight should await HST/STIS spectroscopic observations. Though we derived some information on this in the previous Section using the absorption line residual intensities, the results depend crucially on the assumption that the absorption lines are resolved. We can complement the previous analysis using the total equivalent widths and their ratios without making any assumption about the spectral resolution In addition, when considering total equivalent widths, the consequence of contamination by weak lines is small unlike in the case of the analysis of the residual intensities. The constrains are much weaker however.

Let us assume that the absorption is saturated along line of sight number one and optically thin along line of sight number two. Therefore $W_1^{\rm real}(2796) = W_1^{\rm real}(2803)$ and $W_2^{\rm real}(2796) = 2{\times}W_2^{\rm real}(2803)$. The combined observed equivalent width ratio is:

$$\frac{W^{\rm obs}(2803)}{W^{\rm obs}(2796)} = \frac{\frac{1}{2} + \frac{W_1^{\rm real}(2796)}{W_2^{\rm real}(2796)}\frac{F_1}{F_2}}{1 + \frac{W_1^{\rm real}(2796)}{W_2^{\rm real}(2796)}\frac{F_1}{F_2}} \qquad (4)$$

where F_1 and F_2 are the fractional flux contributions of the two distinct background sources. In Fig. 6, we have plotted $W_1^{\rm real}(2796)$ /$W_2^{\rm real}(2796)$ versus $W^{\rm obs}(2803)$ /$W^{\rm obs}(2796)$ for $F_1/F_2 = 0.65$ (1 is B; 2 is A+C), 1 (1 is A or B+C; 2 is B+C or A) and 1.5 (1 is A+C; 2 is B). The vertical dashed-dotted lines correspond to the observed doublet ratios of the systems at $z_{\rm abs} = 1.221$, 1.5523 and of the reddest component of the $z_{\rm abs} = 1.5497$ system.

From Fig. 6, it can be seen that the $z_{\rm abs} = 1.221$ system (doublet ratio of 0.96) requires the ratio of the equivalent widths of Mg IIλ2796 along the two lines of sight to be larger than 8. and the column densities along the two sightlines differ by more than an order of magnitude.

3.4. Dimension of individual clouds

Rauch et al. (1999) have observed strong variations of C II and Si II absorptions at $z = 3.538$ along two sightlines separated by only $13h^{-1}$ pc. However, as the velocity difference between the quasar and the system is only 6000 km s^{-1}, it cannot be excluded that the latter system is somehow associated with the quasar. Variations of the strength of metal line systems have also been reported along adjacent lines of sight with larger separations (5–10 kpc) by Monier et al. (1998) and Lopez et al. (1999). Each time however a damped Lyman-α system is seen along one of the sightlines. Contrary to these previous studies, the Mg II systems we examine here are most likely to be associated with halos of intervening galaxies.

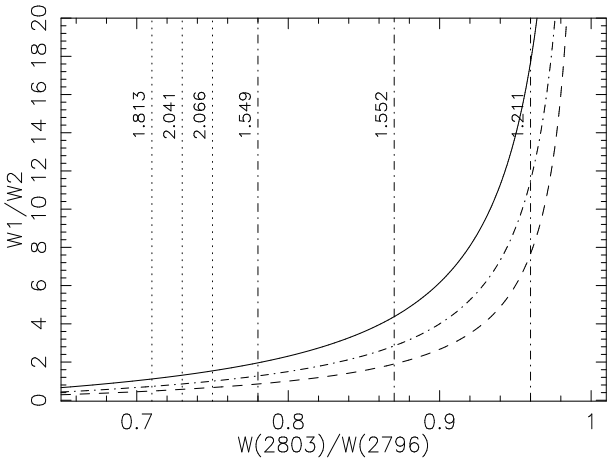

Fig. 6. Equivalent width ratio of the Mg IIλ2796 absorption line along two different line-of-sights 1 and 2 versus the observed doublet ratio for three different flux ratios $F_1/F_2 = 0.65$ (solid line), 1 (dashed-dotted line) and 1.5 (dashed line). The Mg II doublet is assumed to be saturated along line-of-sight 1 and optically thin along line-of-sight 2. The doublet ratios observed for six Mg II systems toward APM 08279+5255 are shown as vertical dashed-dotted and dotted lines for $z_{\rm abs} < 1.5$ and $z_{\rm abs} > 1.5$ respectively. Redshifts are indicated next to the lines.

From the detection of associated galaxies, radii of the order of $35h^{-1}$ kpc have been derived for Mg II halos producing absorptions with equivalent widths $W_{\rm r} > 0.3$ Å at $z < 1$ (Bergeron & Boissé 1991, Steidel 1993). Dimensions of the same order have been derived from the study of Mg II systems seen along two lines of sight separated by 3 arcsec (Smette et al. 1995). The latter authors find a lower limit of 22 h_{50}^{-1} kpc for the radius of Mg II absorbers with $W_{\rm r} > 0.3$ Å at $0.5 < z < 1.3$.

If we assume that the lensing galaxy of APM 08279+5255 is at $z_{\rm lens} \sim 1$ (see next Section), the separation between the two lines of sight to A and B decreases from 1.7 to 0.7 h_{75}^{-1} kpc ($q_{\rm o} = 0.5$) between $z = 1.22$ and $z = 2.04$ and is more than an order of magnitude smaller than the radius of Mg II halos at intermediate redshift. Although evolution is probable, it would be really surprizing that the Mg II systems studied here with $W_{\rm r} < 0.5$ Å at $z_{\rm abs} > 1.2$ have characteristic dimensions more than an order of magnitude smaller than what is derived at lower redshift. If true, this would suggest that the structure of the Mg II halos at these redshifts differs substantially from that at lower redshifts.

A more likely explanation of these observations is that the halos are composed of a collection of clouds (see Petitjean & Bergeron 1990; Srianand & Khare 1994) and that

individual clouds cover only one sight line. The number density of clouds is large enough so that the total covering factor of the halo is close to one, consistent with observations of associated galaxies. However, individual clouds, regularly spread over the velocity profile by kinematics, cover only one image of the lens. The number density of clouds is not large enough for the absorption material to cover the two lines of sight at all velocities. The distance over which the optical depth, and hence the column density of Mg II , changes by at least one order of magnitude at $z_{\rm abs}$<1.7 is smaller than $\sim 1h_{75}^{-1}$ kpc. In contrast, the two strong Mg II systems at $z_{\rm abs} = 1.06$ and 1.18 (see below) have covering factor equal to one (the lines are saturated and go to the zero level) over more than 200 km s^{-1}. These latter systems are likely to arise due to absorption through central regions of galaxies where the number of clouds is so large that saturated absorption occurs along both lines of sight whatever the radius of the individual clouds might be.

4. The two Mg II systems at $z_{\rm abs}$ =1.062 and 1.181

The presence of a strong Mg II system ($W_{\rm r}\lambda2803 \sim 2.4$ Å) at $z_{\rm abs} \sim 1.18$ was already mentioned by Irwin et al. (1998). There is an additional even stronger Mg II system at $z_{\rm abs} = 1.062$ ($W_{\rm r}\lambda2803 \sim 3.3$ Å). Although the Mg II lines are redshifted in the Lyman-α forest and may be blended with Lyman-α intervening absorptions, the existence of the system is confirmed by numerous lines redshifted redward of the quasar Lyman-α emission. As the two brightest images of the lensed quasar have similar magnitudes, it is expected that the lines of sight to both images pass through the core of the lensing object where strong Mg II absorption is likely to occur. The gravitational lensing may thus result from the cumulative effect of the two galaxies associated with these two absorbing systems together with the objects responsible for the possible system at $z_{\rm abs} = 1.1727$ (see Section 3.1) and the other damped Lyα system at $z_{\rm abs} = 2.974$. Absorptions from Mg II, Fe II, Ca II, Mn II, Ti II and Na I are seen in both systems (see Figs. 7,8).

4.1. Na I absorptions

In both Mg II systems, the weak Na I$\lambda\lambda$3303,3303 doublet is detected (see Figs. 7 and 9). The fact that the two lines of the doublet are seen with consistent strengths gives confidence that the identification is correct. We have identified lines from other metal line systems in the vicinity of the doublet. The spectra of APM 08279+5255 and the standard star are compared in Fig. 9 to rule out the possibility that the absorption features are of atmospheric origin.

The column densities obtained by Voigt profile fitting are large, log N(Na I) = 12.9 and 13.5 at, respectively,

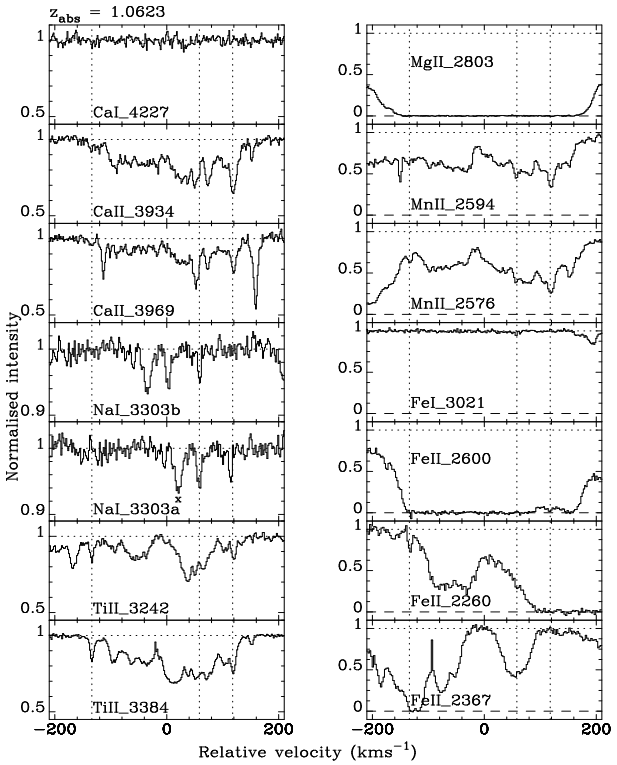

Fig. 7. Absorption in a few transitions on a velocity scale with origin at $z_{\rm abs} = 1.06230$. Vertical dashed lines mark velocity components discussed in the text.

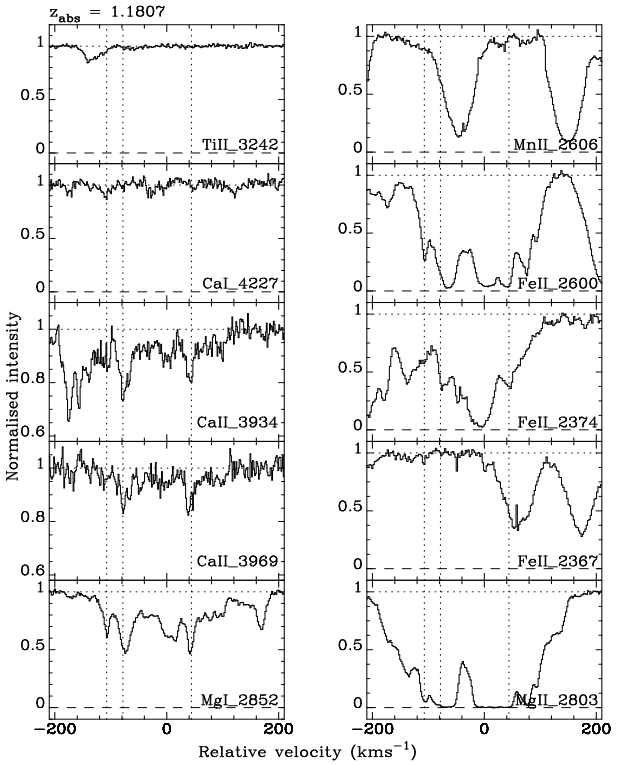

Fig. 8. Absorptions in a few transitions on a velocity scale with origin at $z_{\rm abs} = 1.18070$. Vertical dashed lines mark velocity components discussed in the text.

$z_{\rm abs} = 1.0626$ and 1.1801. The separation of the two principal lines of sight is $\sim 1.9 h_{75}^{-1}$ kpc at $z \sim 1$. It is therefore possible that the clouds seen by their Na I absorptions do not cover the two brightest lines of sight. In that case, however, the column density could be even larger by a factor of two (see Section 4.4).

Using the measurements by Sembach et al. (1993) and Diplas & Savage (1994), Bowen et al. (1995) find that , in our Galaxy, $\log N$(H I) = 0.688 $\log N$(Na I) + 12.16. Note that this correlation holds up to column densities $\log N$(H I) > 21 (see e.g. Ferlet et al. 1985). Applying this correlation for the $z_{\rm abs} = 1.0626$ and 1.1801 absorbers gives neutral hydrogen column densities of the order of $\log N$(H I) $\sim$ 21.0 and 21.4 respectively, for gas-phase metallicities comparable to what is seen in the interstellar medium in our Galaxy (the neutral hydrogen column densities could be even larger if the metallicity in these intermediate-redshift systems is smaller than in our Galaxy). Such large values for N(H I) are supported by the column densities of other species that are found to be surprisingly close to what is observed in typical interstellar clouds (see below and Table 2). This leaves little doubt that the systems are indeed damped Lyman-α systems.

In our Galaxy, such high Na I column densities are seen only in dense and cool gas (see below). The typical b values of the Na I diffuse components in both the local and low-halo gas is about 0.7 km s^{-1} corresponding to $T < 500$ K (Welty et al. 1994). Although the conclusion is very uncertain given the resolution of the spectrum ($R \sim 37500$) and the double nature of the background source, the lines we observe are consistent with b values as small as 1 km s^{-1} (see below). From this, we derive an upper limit on the temperature of $T < 2000$ K.

4.2. Comments on each system

4.2.1. $z_{\rm abs} = 1.062$

A subset of the absorptions detected in this system is shown in Fig. 7. It can be seen that strong (but unsaturated) absorptions from Ti II and Ca II are detected. The profile of the Ti II absorption is spread over about 250 km s^{-1} but does not show any edge leading pattern (Prochaska & Wolfe 1998). We have selected to examine two components at $z_{\rm abs} = 1.0613$ and 1.0631 because they show well detached absorptions in Ti II, Mn II, Ca II and/or Fe II plus the component at $z_{\rm abs} = 1.0626$ in which we see Na I. Column densities are listed in Table 2. We have adjusted the best values for b from the fit to the lines that are free of any blending, considering for simplicity that all species have the same Doppler parameter and assuming complete coverage. We find $b = 1.5$, 1.5 and 1.9 for, respectively, $z_{\rm abs} = 1.0613$, 1.0626 and 1.0631.

Ca I is not detected and the 3σ upper limit on the column density in the three components we have selected is < 10.43, 10.43 and 10.20. The Mg IIλ2796,2803 and Fe II$\lambda\lambda\lambda$2382,2600,2586 lines are badly saturated. Moreover, they are redshifted in the Lymanα forest, which prevents any fit of the lines. However, the unsaturated Fe IIλ2260 features detected at $z_{\rm abs} = 1.0613$ and 1.0626 (see Fig. 7) give a reliable estimate of the Fe II column density, $\log N$(Fe II) = 13.90±0.80 and 14.10±0.80 for $b = 1.5$ km s^{-1}, the continuum being adjusted locally. The non-detection of Fe IIλ2367 at $z_{\rm abs} = 1.0631$ gives an upper limit $\log N$(Fe II) < 14.60.

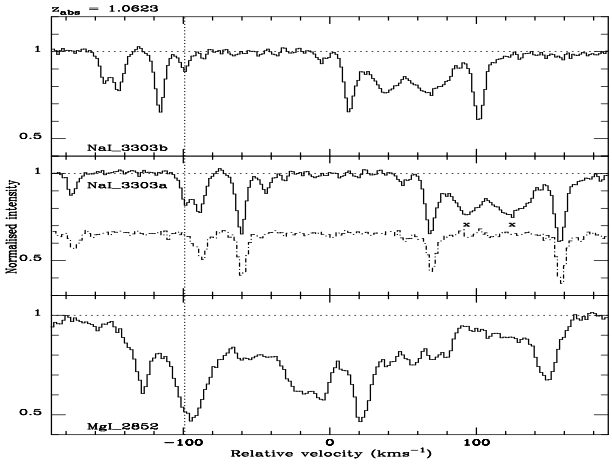

Fig. 9. Portions of the APM 08279+5255 spectrum centered on the expected positions of Na Iλ3303.3 (top panel), Na Iλ3303.9 (middle panel) and Mg Iλ2852 (bottom panel) at $z_{\rm abs} = 1.181$. The Na I component at $z_{\rm abs} = 1.1801$, detected by the two lines of the doublet is indicated by a vertical dashed line. The spectrum of the standard star is overplotted in the middle panel. Metal lines from other systems are indicated by crosses.

4.2.2. $z_{\rm abs} = 1.181$

A subset of the absorptions detected in this system is shown in Fig. 8. The profile of the Mg I absorption is spread over more than 200 km s^{-1} but, as for the previous system, it does not show any edge leading pattern. A number of absorption lines are optically thin or moderately saturated and reliable column densities can be derived even though difficulties arise from most of the components being badly defined (see Fig. 8). We have selected for study two subcomponents which are clearly seen in all absorption profiles at $z_{\rm abs} = 1.1799$ and 1.1801. They are indicated on Fig. 8 by vertical dashed lines, and the column densities obtained from Voigt-profile fitting are given in Table 2. Doppler parameters have been considered to be identical for all species. For $z_{\rm abs} = 1.1799$ we find $b = 2.5$ km s^{-1}.

For the component at $z_{\rm abs} = 1.1801$ in which Na I absorption is detected, the Doppler parameter is estimated by fitting the well-defined lines of the sodium doublet after having taken into account the effect of Na Iλ3303.3 being

partially blended with an atmospheric feature (see Fig. 9). We obtain a best value $b = 1.1^{+1.0}_{-0.5}$ km s^{-1}. The column densities derived using the two values $b\pm 1\sigma$ differ by large factors. We have therefore refined the determination of b and N using the following indirect argument.

The ratio of the Mg I to the Na I column densities in neutral gas can be written

$$\frac{N(\text{Mg I})}{N(\text{Na I})} = \frac{\text{Mg I}}{\text{Mg}} \times \frac{\text{Na}}{\text{Na I}} \times \frac{\delta_{\text{Mg}}}{\delta_{\text{Na}}} \times \frac{Z_{\text{Mg}}}{Z_{\text{Na}}}, \quad (5)$$

where δ is the depletion of the element due to the presence of dust and Z the abundance. Assuming that (i) the relative abundance of Na to Mg is solar, $Z_{\text{Mg}}/Z_{\text{Na}} = 19$, (ii) the relative depletion into dust-grains is $\delta_{\text{Mg}}/\delta_{\text{Na}} > 0.3$ (Savage & Sembach 1996) and (iii) (Mg I/Mg II)×(Na II/Na I) > 0.15 in cold and neutral gas (Péquignot & Aldrovandi 1986), we derive $N(\text{Mg I})/N(\text{Na I}) \geq 0.8$. This estimation is certainly very approximate. However, this simple argument shows that the latter ratio cannot be much smaller than 0.5. If we assume $b = 1.5$ km s^{-1}, then we find $N(\text{Mg I})/N(\text{Na I}) = 0.045$ which is definitively too small. We therefore have fitted the absorption lines decreasing b from 1.5 to 0.5 km s^{-1} to find the largest $N(\text{Mg I})/N(\text{Na I})$ ratio. We find a maximum $N(\text{Mg I})/N(\text{Na I}) = 0.3$ for $b = 0.8$ km s^{-1}, log N(Mg I) = 13.0 and log N(Na I) = 13.5.

4.3. Physical state of the gas

Table 2 contains the column densities measured in the five subcomponents defined above. The penultimate column gives for comparison the column densities measured by Welty et al. (1999) in the neutral gas toward 23 Ori. This gas is found to have temperature $T \sim 100$ K, hydrogen density $n_{\text{H}} \sim 10$–15 cm^{-3} (and therefore total thickness of 12–16 pc) and electronic density $n_{\text{e}} \sim 0.15\pm0.05$ cm^{-3}. The last column of Table 2 gives the measurements for the strongest component of the warm neutral gas toward μCol (Howk & Savage 1999). This gas is found to have $T \sim 6000$–7000 K and $n_{\text{e}} \sim 0.3$ cm^{-3}. The two sets of column densities are similar except for N(Na I) which is much smaller toward μCol. This illustrates directly that at least in the component at $z \sim 1.1802$ toward APM 08579+5255 where Na I is detected, the gas is most likely to be neutral and cold. Moreover, note also that in our Galaxy, a ratio $N(\text{Na I})/N(\text{Ca II}) > 1$, as observed at $z_{\text{abs}} = 1.1802$ toward APM 08579+5255, is characteristic of cold gas in the disk. Indeed, along the line of sight to the LMC, such large ratios are observed only at the systemic velocities of the LMC and the Galaxy; gas in between has $N(\text{Na I})/N(\text{Ca II}) < 1$ (Vidal-Madjar et al. 1987, Vladilo et al. 1993).

From the upper limit on Ca I and Fe I we can derive, in the components where N(Ca II) and N(Fe II) are measured, a lower limit for the electronic density for a given ionizing field. Indeed, $n_{\text{e}} = (X^{\text{o}}/X^{+})\times(\Gamma/\alpha)$, where Γ is the photoionization rate and α the recombination coefficient. The corresponding electronic densities for a Galactic ionizing field (Péquignot & Aldrovandi 1986), are $n_{\text{e}} < 0.13$ and 3 cm^{-3} for Fe and Ca at $z_{\text{abs}} = 1.0626$ and 1.1801 respectively. Note that the determination of n_{e} in the interstellar medium from the ratio of singly ionized to neutral species is highly uncertain probably because of contamination of the singly ionized column density determination by adjacent components (Welty et al. 1999). Writing the same relation for sodium and equating the expression of n_{e} obtained for sodium and iron or calcium leads to upper limits on the Na I/Na II ratio which depends only on the shape of the ionizing spectrum and not on its absolute value. With the only assumption that the ionizing spectrum has the same shape as in our Galaxy and using the coefficients derived from Péquignot & Aldrovandi (1986; see Welty et al. 1999), we find log Na I/Na II < -1.3 and 0.1 from the constraints obtained on Fe and Ca in the 1.0626 and 1.1801 systems respectively.

From N(H I) = N(Na I)×(Na/Na I)/Z(Na) and using the two upper limits on the Na I/Na II ratios derived above, we can write N(H I) > 19.9 and $19.5/(Z(\text{Na})/Z_{\odot}(\text{Na}))/\delta(\text{Na})$ at $z_{\text{abs}} = 1.0626$ and 1.1801 respectively, where δ(Na) is the fraction of sodium remaining in the gas phase after depletion into dust-grains. This factor is equal to about 0.1 in the ISM (Savage & Sembach 1996). This adds support to arguments presented previously that these systems are damped. To illustrate the discussion, simple photo-ionization models using the code Cloudy (Ferland 1996) have been constructed. The absorbing cloud is modelled as a plane parallel slab with uniform density, solar chemical composition and neutral hydrogen column density 5×10^{20} cm^{-2}. The elements are considered to be depleted into dust-grains as in the cool cloud observed toward ζOph (Savage & Sembach 1996). The shape of the UV flux is taken to be a power-law $F_{\nu} \propto \nu^{-1.0}$. The resulting column densities of various species along a line-of-sight perpendicular to the slab are given versus the ionizing parameter in Fig. 10. As discussed above, the $N(\text{Mg I})/N(\text{Na I})$ ratio can be smaller than one only if magnesium is more depleted into dust grains than sodium. Note that every model that produces enough Na I has temperature less than 100 K.

Finally, we do not detect any CHλ4300 and CH$^{+}\lambda$4232 absorption. The limits on the column densities are log N(CH) < 13.5 and log N(CH^{+}) < 13.0 at both $z_{\text{abs}} = 1.06$ and 1.18 (see Table 2). This is just what would be expected in our Galaxy along an otherwise similar line of sight. Indeed, along the line of sight to 23 Ori, log N(CH^{+}) = 13.06 and log N(CH) = 12.69 (Welty et al. 1999; see Table 2). More generally, the column density of CH is observed to increase from 1.5 to 7.5×10^{13} cm^{-2} for lines of sight with $E_{\text{B}-\text{V}}$ increasing from 0.5 to 1.5 (Gredel et al. 1993). It would be of prime interest to obtain

Table 2. Column densities[a]

Redshift	1.0613	1.0626	1.0631	1.1799	1.1801	23 Ori[b]	μCol[d]
H I						20.74	19.86
H_2						18.30	15.50
Na I	<11.90	12.91±0.04	<12.80	<12.40	13.50±0.11	13.36	11.6[e]
Mg I	11.6:[c]	bl	bl	11.61±0.06	13.0±0.74	13.81	12.55
Mg II						15.68	15.08
Ca I	<10.43	<10.43	<10.20	<10.80	<10.33	10.20	
Ca II	11.31±0.11	bl	11.71±0.03	11.33±0.39	11.79±0.35	12.10	12.19
Ti II	11.80±0.05	<12.00	11.90±0.02	<11.66	<11.20	11.23	11.78
Mn II	bl	bl	12.70±0.40[c]	bl	bl	13.15	12.48
Fe I	<11.50	<11.63	<11.40	<11.40	<11.50	11.34	
Fe II	13.90±0.80	<14.10	<14.60	13.36±0.07	<15.00	14.38	14.13
CH+	<12.80	<12.70	<13.00	<13.20	<13.30	13.06	
CH	<13.40	<13.60	<13.50	<13.40	<13.60	12.69	

[a] logarithm of, in cm^{-2}; Doppler parameters are taken to be b = 1.5, 1.5, 1.9, 2.5, 0.8 km s^{-1} for the five components respectively; the components are assumed to cover all images;
[b]Welty et al. (1999); [c]The continuum is fitted locally; [d] Howk et al. (1999); [e] Hobbs (1978).
A sign "bl" means that no measurement is possible due to blending effects

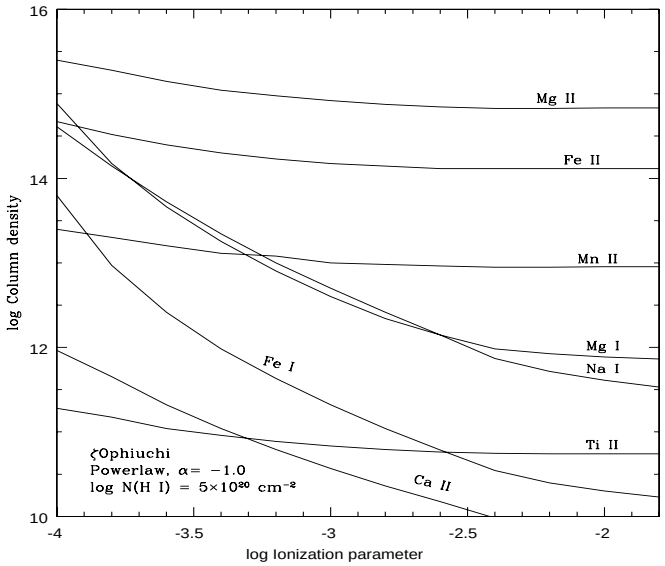

Fig. 10. Results of photoionization models with $Z = Z_{\odot}$, log N(H I) = 20.7, constant density and plane parallel geometry. Depletion into dust-grains is assumed to be the same as in the cool cloud toward ζOph (Savage & Sembach 1996). Column densities are given versus ionization parameter; the shape of the UV flux is a power-law $F_{\nu} \propto \nu^{-1.0}$.

better data in this wavelength range to better constrain the molecule column densities.

4.4. Consequence of partial covering factor

From the detection of the Na I λλ3303.3,3303.9 doublet, we can derive that the two components at $z_{\rm abs}$ = 1.0626 and 1.1801 arise in cold, dense and neutral gas (see Section 4.3). It is therefore possible that the dimension of the cloud is less than ∼1.9 kpc which is the separation of the lines of sight to the two brightest images at the redshift of the absorber assuming that the lensing object is at the same redshift. Indeed, large variations of Na I column density have been reported in the nearby interstellar medium on very small scales (Meyer & Lauroesch 1999). We have therefore investigated the impact on the column density measurements of the assumption that the cloud covers the three images. If it is the case that the cloud covers only one of the images the column density is larger. The discrepancy cannot be very large, however, as most of the lines used for column density determination are weak. The strong lines are completely saturated and blended, which prevents in any case any determination of the line parameters.

We have considered the Mg I and Na I lines in the $z_{\rm abs}$ = 1.1801 component. It can be seen on Fig. 8 that if only one image is covered, it cannot be the brightest as the residual normalized flux in the Mg I absorption is smaller than 0.5. As the flux ratio of the two brightest components is 1.2, we artificially placed the zero level at 0.4 on the scale of Fig. 8. Voigt profile fitting of the Na I doublet gives log N(Na I) = 13.7 and b = 1 km s^{-1} which is within a factor of two of what has been derived previously (see Table 2). Four components have been used to fit the Mg I blend at $\Delta v = -60$ km s^{-1} (see Fig. 8). For the component at $z_{\rm abs}$ = 1.1801, we obtain log N(Mg I) = 13.8.

Note that in this case, the Na I and Mg I column densities are nearly identical to what is observed toward 23 Ori (see Table 2). We therefore conclude that N(Mg I)/N(Na I) ∼ 1 is a robust measurement in this system.

Mg I is the line with the largest saturation among those used to derive column densities quoted in Table 2. Therefore, the column densities derived from weaker lines should not differ from what is quoted in Table 2 by more than a factor of two.

4.5. Metallicity and dust content

In the following we use the conventional definition [X/H] = $\log(Z/Z_\odot)$, with Z(X) the metallicity of species X relative to hydrogen. Ca II and Ti II are both detected at $z_{\rm abs}$ = 1.0613 and 1.0631. The column densities are consistent with what is seen in the interstellar medium of our Galaxy (Stokes 1978; see Table 2). However, log N(Ca II)/N(Ti II) ~ -0.5 and -0.2 at, respectively, $z_{\rm abs}$ = 1.0613 and 1.0631 when the relative solar metallicity is log $Z_\odot$(Ca) − log $Z_\odot$(Ti) = 1.38. Various explanations for this discrepancy can be invoked, amongst them the most likely are: (i) Calcium is mostly in the form of Ca III, (ii) Calcium is more depleted into dust-grains than Titanium. Note that the relative metallicities [Ca/Fe] and [Ti/Fe] are both observed to be $\sim$+0.3 for [Fe/H] < -1 in late-type stars (Thévenin 1998). Note also that the Ca III/Ca II ratio derived in our Galaxy is in the range 5–10 which is much smaller than the discrepancy mentioned above. This favors the explanation that Calcium is heavily depleted into dust-grains (see below).

In the $z_{\rm abs}$ = 1.0631 component, Mn II is also seen and log N(Mn II)/N(Ti II) $\sim$ +0.8. As the solar metallicity of Mn is −6.47, the relative solar metallicity is log $Z_\odot$(Mn) − log $Z_\odot$(Ti) = = +0.6. This is consistent with similar depletion of Mn and Ti as observed in warm gas (Savage & Sembach 1996). Therefore, in this component, we cannot rule out that the low Ca II column density is due to ionization.

In the $z_{\rm abs}$ = 1.0613 component, Fe II is also seen with log N(Fe II)/N(Ti II) $\sim$ +2.1. The solar metallicity of iron and titanium are, respectively, −4.49 and −7.07 and the relative solar metallicity is log $Z_\odot$(Fe) − log $Z_\odot$(Ti) = +2.58. There is no differential ionization correction for these two elements. The discrepancy, $\sim$+0.5 dex, between the two ratios can only be explained by a larger depletion of titanium compared to iron into dust-grains by $\sim$0.5 dex as in the cool gas of the ISM (Savage & Sembach 1996). Indeed, from nucleosynthesis alone, we would expect titanium to be enhanced compared to iron (Thévenin 1998) contrary to what is observed. We therefore conclude that depletion into dust-grains is present in this system. The low Ca II column density can indeed be explained by a large depletion of calcium into dust-grains as is observed in the ISM.

The fact that Ti II is not detected in the $z_{\rm abs} = 1.18$ system is surprising, although the limit on the column density is not stringent and only a factor of four smaller than what is seen in the $z_{\rm abs}$ = 1.06 components.

The presence of dust is supported by the analysis of the column density ratios in the $z_{\rm abs}$ = 1.0626 and 1.1801 components where Na I absorption is detected. Indeed, we can compute for different elements the quantity $N_\odot = 10^{[X/H]} \times N$(H I) which is the H I column density of a cloud with solar metallicity that would have the same column density of element X as the observed one. We compute,

$$\log N_\odot = [{\rm X/H}] + \log N({\rm HI}) = \log\left(N({\rm X}^i) \frac{\rm X}{{\rm X}^i} \frac{1}{\delta} \frac{1}{Z_\odot({\rm X})} \right) \quad (6)$$

where $Z_\odot$ is the solar metallicity and 1-δ the fraction of the element tied up into dust-grains. We assume solar metallicity and depletion pattern given in Table 5 of Savage & Sembach (1996). Solar metallicities relative to hydrogen for Na, Fe, Ca and Ti are, respectively, −5.69, −4.49, −5.66 and −7.07. If we assume that the absorption arises in cool gas similar to the gas seen in front of ζOph, we find that at $z_{\rm abs}$ = 1.1801, log $N_\odot$ >20.44, <21.80, <21.18, <21.30 from Na, Fe, Ca and Ti and at $z_{\rm abs}$ = 1.0626, log $N_\odot$ >20.85, = 20.86, <22.10 from Na, Fe and Ti respectively.

These consistent results suggest that, in the $z_{\rm abs}$ = 1.0626 and 1.1801 components, log N(H I) + [X/H] $\sim$ 21 and the depletion into dust-grains is similar to what is seen in cool Galactic interstellar clouds. If the relation of Bohlin et al. (1978) holds, this implies a color excess $E_{\rm B-V} \sim 0.2$ with the only assumption that the overall dust-to-metal ratio does not depend on metallicity. At the wavelength of the Mg II absorption, ($\lambda_{z=1} \sim 3000$ Å; $\lambda_{\rm rest}^{\rm QSO} \sim 1200$ Å; $\nu_{\rm rest}^{\rm QSO} \sim 2\times10^{15}$ Hz) this would induce an extinction of about 1 mag (Seaton 1979). At $\nu_{\rm rest}^{\rm QSO} \sim 10^{14}$ Hz, the extinction would be negligible. Note that there is some evidence that νF_ν decreases by a factor of two from 10^{15} to 10^{14} Hz in the APM 08279+5255 SED (Lewis et al. 1998).

The amount of dust suggested by the previous discussion is significant. We have therefore searched the spectrum of the quasar for some signature of this amount of dust. For this, we have compared the spectrum of APM 08279+5255 with the composite QSO spectrum obtained with the FOS-HST (Zheng et al. 1997) attenuated by dust with optical depth $\tau_{\rm dust}(\lambda)$ at the observed wavelength λ,

$$\tau_{\rm dust}(\lambda) \;=\; k \left[\frac{N}{10^{21}{\rm cm}^{-2}} \right] \xi\left(\frac{\lambda}{1+z} \right) \quad (7)$$

where $\xi(\lambda)$ is the ratio of the extinction at the wavelength λ to that in the B-band as observed in our Galaxy, $k = 10^{21}$ cm^{-2} $\tau_{\rm B}/N$(H I) is the dimensionless dust-to-gas ratio and N the H I column density (e.g. Pei et al. 1991, Srianand & Kembhavi 1997). We assume here log N(H I) = 21. The redshift of the QSO is taken to be $z_{\rm QSO}$ = 3.91 and that of the absorber $z_{\rm abs}$ = 1.1. The results are shown in Fig. 11 where the spectrum of APM 08279+5255 as observed over part of the R-band

(solid line) is plotted together with the composite HST-FOS QSO spectrum attenuated by dust with optical depth in the B-band $\tau_{\rm dust}(\rm B) = 0.1$, 0.2 and 0.3. It is apparent that the best fit is obtained with $\tau_{\rm dust}(\rm B) \sim 0.3$. In our Galaxy, this would correspond to about $E_{\rm B-V} \sim 0.1$. This is two times smaller than what has been derived above. This suggests that the dust to metal ratio in the redshifted gas is about half that in our Galaxy.

Altogether we find that the H I column density at $z = 1$ is of the order of 1×10^{21} cm^{-2} to 5×10^{21} cm^{-2}, the corresponding metallicity is in the range 1–0.3 $Z_{\odot}$, the dust-to-metal ratio is about half that in our Galaxy and the relative depletion of species into dust-grains is similar to what is observed in cool gas in the disk of our Galaxy.

The colors of the images derived from HST imaging are nearly identical (Ibata et al. 1999). The differential reddening over kpc scales is smaller than 10%. This indicates that, although the medium is highly inhomogeneous, the extinction is fairly uniform over distances of the order of the separation between the lines of sight. It must be noted that the number of components in the two strong Mg II systems must be quite large. Indeed, the Mg II absorptions reach the zero level over ∼200 and 350 km s^{-1} at, respectively, $z_{\rm abs} = 1.181$ and 1.062. One single component cannot be much larger than about ∼10 km s^{-1} and therefore the number of components is larger than 20 and 40 respectively along all three lines of sight. This is probably larger than what is seen in the disk of our Galaxy (Sembach & Danks 1994). Therefore, it may well be possible that the total reddening we see is not due to one strong component only but rather is due to the accumulated effect of a large number of diffuse clouds with small and similar extinctions. As the number of clouds is large and similar along the different lines of sight, the differential extinction is small. To probe this, higher S/N ratio data should be obtained in the region of the Na I absorption to investigate what is the velocity spread of this absorption.

4.6. Nature of the systems

Churchill (1999) has shown that Mg II systems at intermediate redshift can be classified in five categories: DLA, Double, Classic, C IV deficient and Weak. The first class is characterized by strong Mg II absorption saturated over ∼150 km s^{-1} and, when observed, the Lyman-α line is damped. The Double systems are characterized by kinematic velocity spreads up to 400 km s^{-1}. Other classes correspond to much weaker systems.

The system at $z_{\rm abs} = 1.181$ would be classified as Double (see Fig. 8): it has Mg IIλ2796 absorption saturated over more than 150 km s^{-1} in total. The characteristic double profile is very similar to that of the system at $z_{\rm abs} = 1.17$ toward Q 0450–132 (see Petitjean et al. 1994). The system at $z_{\rm abs} = 1.062$ would be classified as DLA, as the Mg II absorption is continuously saturated over more than 300 km s^{-1} (see Fig. 7). To our knowledge, this system has one of the strongest Mg II absorption features known ($W_{\rm r} \sim 3.3$ Å). As seen from Fig. 7, the Ti II absorption spans ∼ 300 km s^{-1} and coincides exactly with the saturated part of the Mg II absorption.

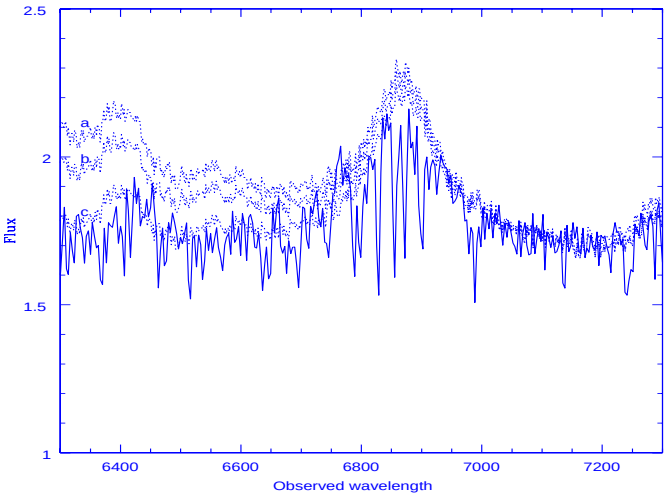

Fig. 11. Spectrum of APM 08279+5255 as observed over part of the R-band (solid line) plotted together with the composite QSO spectrum obtained from FOS-HST observations (Zheng et al. 1997) and attenuated by dust with optical depth in the B-band, $\tau_{\rm dust}(\rm B) = 0.1$ (a), 0.2 (b) and 0.3 (c; see text). The Galactic extinction curve is assumed.

At high-z, Prochaska & Wolfe (1998) have shown that most of the low-ionization absorptions associated with DLAs, have an edge-leading profile, possibly revealing large-scale rotational motions. They conclude that DLA systems arise in large rotating disks. Haehnelt et al. (1998) have claimed that the observed profiles can be reproduced as well if the line of sight passes through several interacting blobs. Indeed, Ledoux et al. (1998a) have shown that the observed profiles are consistent with rotation when they span less than $\Delta V \sim 150$ km s^{-1}. For larger velocity spreads, several sub-systems are usually seen.

The characteristic edge-leading profile is seen in the $z_{\rm abs} = 2.974$ system (see below, Fig. 12) but not in the $z_{\rm abs} = 1.062$ and 1.181 Mg II systems. The large spread of the profiles (> 200 and 300 km s^{-1}) is more reminiscent of the profile seen toward the supernova SN 1993J in the large nearby spiral galaxy M 81. The latter is part of a complex interacting group together with M 82, NGC 3077 and NGC 2976 with tidally stripped H I linking individual galaxies over an area of ∼50×100 kpc^2 (Yun et al. 1994). The Mg II absorption is characteristic of the Double class as defined by Churchill (1999). It is spread over ∼400 km s^{-1} with two strong saturated absorptions of width, respectively, $\Delta V \sim 150$ and 90 km s^{-1}, and separated by ∼180 km s^{-1} (Bowen et al. 1995). Most of the

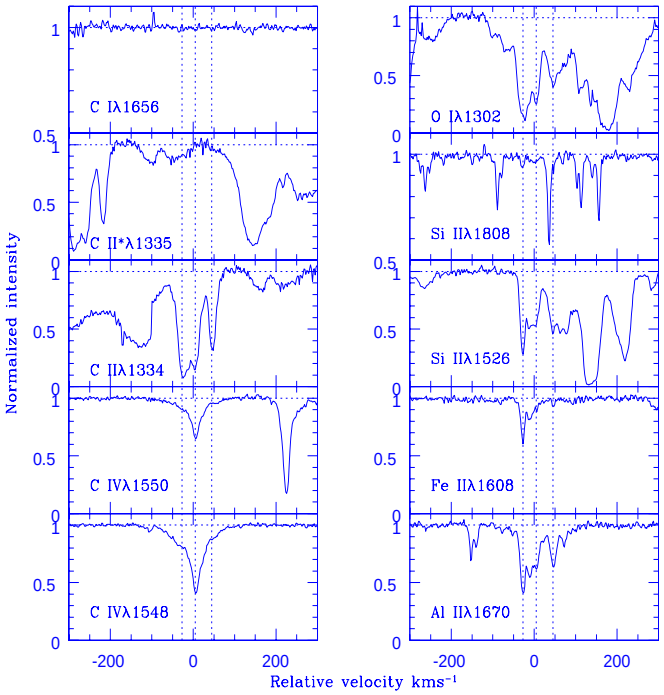

Fig. 12. Absorptions in a few transitions on a velocity scale with origin at $z_{\rm abs} = 2.974$. Vertical dashed lines mark the position of the strongest components.

absorption is due to tidal debris expelled outside the disks of the interacting galaxies.

In the case of the $z_{\rm abs} = 1.062$ system, the Mg II absorption does not show any sub-structure. Such strong absorption is expected to occur in the central part of galaxies. Although the statistics are very poor, it seems that when strong absorption occurs, the equivalent width of the absorption is anti-correlated with the impact parameter between the line of sight and the center of the galaxy (Bowen et al. 1995). The impact parameter could be as low as 1 kpc for a system with $W_{\rm r} \sim 3$ Å. The separation between the two bright images of APM 08279+5255 is $\sim 1.9 h_{75}^{-1}$ kpc at $z \sim 1$. This suggests that the object giving rise to the $z_{\rm abs} = 1.06$ Mg II system could be nearly exactly aligned with the quasar.

5. The system at $z_{\rm abs} = 2.974$

There is a strong absorption feature with $W_{\rm obs} > 19$ Å at $\lambda = 4831$ Å. It corresponds to H I Lyman-α at $z_{\rm abs} = 2.974$. The only possibility of coincidence with a BAL transition could be Lymanβ at $z_{\rm abs} = 3.71$ but there is no corresponding Lymanα transition (see Srianand & Petitjean 2000). Although the red-wing of the absorption has the characteristic shape of a damped transition, uncertainties in the continuum determination prevent an accurate determination of the column density. Associated absorptions from Al II, Fe II, Si II, C II and O I are detected in four components spanning ∼100 km s^{-1} (see Fig. 12). By fitting the Lyman-α line, we estimate that the total H I column density in the four components is in the range $19.8 < \log N({\rm H\ I}) < 20.3$.

It is important to note that there is no evidence that the cloud does not cover the three lines of sight which are separated by $\sim 200 h_{75}^{-1}$ pc at the redshift of the absorber. Indeed, the core of the H I absorption is black over ~ 15 Å. Column densities integrated over the absorption profiles have been obtained for all species and summarized in Table 3. Column #3 of Table 3 gives the abundance of the element assuming that $\log N({\rm H\ I}) = 20.3$ in the cloud and that the observed ion is the dominant species. Given the uncertainty in the neutral hydrogen column density, the absolute values are unreliable and could be 0.5 dex higher. Column #4 and #5 of Table 3 give the solar metallicity and the metallicity relative to solar respectively. It is remarkable how consistent the measurements are, which point toward metallicities less than $10^{-1.5}$ $Z_\odot$. The low metallicities are not due to depletion into dust-grains. Indeed, the relatively small neutral hydrogen column density implies that column densities of relatively abundant elements can be measured. It is apparent that iron is not depleted compared to carbon or oxygen and that the amount of dust in this cloud must be very small.

Metallicity in damped Lyman-α systems is usually measured using zinc, an element that is not very much depleted into dust-grains in our Galaxy and, because it has relatively low metallicity compared to other elements, induces non-saturated absorptions even for clouds of high hydrogen column density. There is barely no evolution in the measured Zinc metallicity from $z \sim 1$ to $z \sim 3$ (Pettini et al. 1997, 1999). At $z > 3$, in most damped Lyman-α studied up to now, zinc is not detected. This is most probably a consequence of limited S/N ratio of the data however. Indeed, the detection limit of most of the spectra is $\log N({\rm Zn\ II}) \sim 11.5$ which means [Zn/H] < -1.4 (see e.g. Prochaska & Wolfe 1997). It can be noted that in the system at $z_{\rm abs} = 2.974$ toward APM 08279+5255, the limit on zinc is of this order. However, as we can measure metallicities for more abundant elements, we know that metallicities are less than -1.5. For such abundances, zinc would have been detectable in the spectrum of APM 08279+5255 only for H I column densities larger than 10^{21} cm^{-2}. It is therefore possible that the upper limit found for the zinc metallicity at $z > 3$ in previous surveys is indicative of a true evolution of the metallicity in individual systems (see also Prochaska & Wolfe 2000; Savaglio et al. 1999). This should be checked by measuring in the same systems abundances of species like carbon, aluminium, silicon and iron.

Table 3. Column densities[a] in the $z_{\rm abs} = 2.974$ system

Species	log N ($\rm cm^{-2}$)	Z^b	$Z_\odot$	[X/H][b,c]
H I	19.8–20.3			
C II	14.5	−5.80	−3.45	−2.35
O I	14.8:	−5.50	−3.13	−2.37
Al II	12.5	−7.78	−5.52	−2.26
Si II	13.8	−6.55	−4.45	−2.10
Fe II	13.5	−6.80	−4.49	−2.31
Zn II	<11.8	< −8.50	−7.35	< −1.1
Ni II	<12.5	< −7.80	−5.75	< −2.0

[a] logarithm of, in $\rm cm^{-2}$; [b] log N (H I) = 20.3 is assumed; [c] typical errors are ±0.3 dex.

6. Conclusion

The doublet ratio of several intervening Mg II$\lambda\lambda$2796,2803 systems along the line of sight to APM 08279+5255 is observed close to unity, indicating saturation of the lines, whereas the depth of the lines is close to 0.5 in the normalized spectrum (see Fig. 1). This can be understood if the absorption profile is made of components with arbitrarily small Doppler parameters ($b \sim$ 1–1.5 km $\rm s^{-1}$). This would imply however a surprisingly low temperature (1500–3000 K) when the gas is expected to be heated by photo-ionization to temperatures larger than 10^4 K (e.g. Petitjean et al. 1992). A more likely explanation of these observations is that Mg II galactic halos are composed of a collection of clouds each of them having dimensions less than ∼1 kpc. Individual clouds, regularly spread over the velocity profile by kinematics, cover only one of the two brighest image of the lensed quasar. The number density of clouds is not large enough for the absorption material to cover the two lines of sight at all velocity positions. The total covering factor of the halo however is close to one, consistent with observations of associated galaxies at intermediate redshift. In contrast, the two strong Mg II systems at $z_{\rm abs} = 1.06$ and 1.18 have covering factor equal to one (the lines are saturated and go to the zero level) over more than 200 km $\rm s^{-1}$. These latter systems are likely to arise due to absorption through the central part of galaxies where the number of clouds is so large that saturated absorption occurs along both lines of sight whatever the radius of the individual clouds might be.

Models by Mo & Miralda-Escudé (1996) have shown that halos with small rotation velocity (< 100 km $\rm s^{-1}$) should contribute little to the total cross-section of Mg II systems as they have dimensions as small as 5 kpc. This conclusion is probably true at $z < 1$ (see also Churchill et al. 1996). It is however interesting to note that most of the $z > 1$ Mg II systems studied here (see Fig. 1) are spread over much less than 100 km $\rm s^{-1}$. Moreover, they have equivalent widths $W_{\rm r} \sim$ 0.43, 0.37, 0.12, 0.99, 0.28 and 0.17 Å at $z_{\rm abs} = 1.211$, 1.5497, 1.5523, 1.813, 2.0418 and 2.0668 respectively. Therefore the systems we see have similar strengths as the systems which, at lower redshift, are associated with large halos of galaxies. In particular, they are generally stronger than the weak Mg II systems studied by Churchill et al. (1999). This means that, contrary to what is seen at lower redshift, these systems could be associated with halos of low rotation velocity (< 100 km $\rm s^{-1}$) and thus small radii.

The two strong Mg II systems at $z_{\rm abs} = 1.06$ and 1.18 are studied in detail. Absorption from Ca II, Mg I, Ti II, Mn II and Fe II have been observed in several damped Lyman-α systems over a large range of redshift (Meyer et al. 1995, Lu et al. 1996, Vladilo et al. 1997, Proschaska & Wolfe 1997, Churchill et al. 2000). This is, however, the first time that Na I is also detected at such redshift, thanks to the combination of high S/N ratio and high spectral resolution. This additional strong constraint shows that the gas in these systems is cool and neutral. Indeed, similar column densities are observed in our Galaxy for Ca II, Mg I, Ti II, Mn II and Fe II in warm and cool gas clouds toward, respectively, μCol and 23 Ori. Only the Na I column density differs; it is more than an order of magnitude larger through the cool cloud. Doppler parameters as low as $b \sim 1$ km $\rm s^{-1}$ are derived from Voigt-profile fitting of isolated subcomponents. We find that the H I column density at $z = 1$ is of the order of 1×10^{21} $\rm cm^{-2}$ to 5×10^{21} $\rm cm^{-2}$, the corresponding metallicity is in the range 1–0.3 $Z_\odot$, the dust-to-metal ratio is about a third that in our Galaxy and the relative depletions of iron, titanium, manganese and calcium are similar to those in cool gas in the disk of our Galaxy. The dust-to-metal ratio measured here is similar to what is derived in most of the damped Lyman-α systems (Vladilo 1998, Savaglio et al. 1999). The presence of dust is supported by the reddening of the QSO spectrum over the R-band. These are probably amongst the most metal and dust-rich damped Lyman-α systems at $z \sim 1$. The dust depletion pattern is similar to that observed in cool gas in the Galaxy. All this is consistent with the finding by Petitjean et al. (1992) that although most of the damped Lyman-α systems arise in warm gas, the highest column densities are due to a collection of clumps that condense out of the warm phase due to thermal instability (see also Lane et al. 2000).

Another damped Lyman-α system is seen at $z_{\rm abs} = 2.974$ with $19.8 <$ log N(H I) < 20.3. As the Lyman-α line is black over about 15 Å, the cloud must cover the three QSO images. The transverse dimension of the absorber is therefore larger than 200 h_{75}^{-1} pc. Column densities of Al II, Fe II, Si II, C II and O I indicate abundances relative to solar of −2.31, −2.26, −2.10, −2.35 and −2.37 for, respectively, Fe, Al, Si, C and O (for log N(H I) = 20.3). Metallicities are therefore less than $10^{-1.5}$ $Z_\odot$ and, if any, the amount of dust in the cloud is very small, as are any deviations from relative solar abundances. It seems likely that the difficulty to detect Zinc in several damped Lyman-α systems at $z > 3$ in previous surveys is indicative of a true cosmological evolution of the metallicity in individual systems (see also Prochaska &

Wolfe 2000, Savaglio et al. 1999). This should be checked by measuring in the same systems abundances of species like carbon, aluminium, silicon and iron.

Acknowledgements. We thank the team headed by Sara L. Ellison to have made this beautiful data available for general public use and particularly Sara L. Ellison for an access to individual spectra. We gratefully acknowledge support from the Indo-French Centre for the Promotion of Advanced Research (Centre Franco-Indien pour la Promotion de la Recherche Avancée) under contract No. 1710-1. PPJ thanks Elisabeth Flam for useful discussions and Patrick Boissé for a critical reading of the manuscript.

References

Bergeron J., Boissé P., 1991, A&A 243, 344
Bohlin R.C., Savage B.D., Drake J.F., 1978, ApJ 224, 132
Bowen D.V., Blades J.C., Pettini M., 1995, ApJ 448, 634
Carswell R.F., Webb J.K., Baldwin J.A., Atwood B., 1987, ApJ 319, 709
Churchill C.W., 1999, astro-ph/9909426
Churchill C.W., Mellon R.R., Charlton J.C., et al., 2000, ApJ submitted
Churchill C.W., Rigby J.R., Charlton J.C., Vogt S.S., 1999, ApJS 120, 51
Churchill C.W., Steidel C.C., Vogt S.S., 1996, ApJ 471, 164
Diplas A., Savage B.D., 1994, ApJS 93, 211
Ellison S.L., Lewis G.F., Pettini M., et al. 1999a, PASP 111, 946
Ellison S.L., Lewis G.F., Pettini M., et al. 1999b, ApJ 520, 456
Elvis M., Wilkes B.J., McDowell J.C., et al., 1994, ApJS 95, 1
Ferland, G. J. 1996, "HAZY a Brief Introduction to Cloudy", Univ. Kentucky, Dept. Physics & Astron.. Internal rep.
Ferlet R., Vidal-Madjar A., Gry C., 1985, ApJ 298, 838
Fontana A., Ballester P., 1995, The Messenger 80, 37
Gredel R., van Dishoeck E.F., Black J.H., 1993, A&A 269, 477
Haehnelt M.G., Steinmetz M., Rauch M., 1998, ApJ 495, 647
Hobbs L.M., 1978, ApJ 222, 491
Howk J.C., Savage B.D., Fabian D., 1999, ApJ 525, 253
Ibata R.A., Lewis G.F., Irwin M.J., Lehár J., Totten E.J., 1999, AJ 118, 1922
Irwin M.J., Ibata R.A., Lewis G.F., Totten E.J., 1998, ApJ 505, 529
Lane W.M., Briggs F.H., Smette A., 2000, ApJ 532, L146
Ledoux C., Petitjean P., Bergeron J., Wampler E.J., Srianand R., 1998a, A&A 337, 51
Ledoux C., Thédore B., Petitjean P., et al., 1998b, A&A 339, L77
Lespine Y., Petitjean P., 1997, A&A 317, 416
Lewis G.F., Chapman S.C., Ibata R.A., Irwin M.J., Totten E.J., 1998, ApJ 505, L1
Lopez S., Reimers D., Rauch M., Sargent W.L.W., Smette A., 1999, ApJ 513, 598
Lu L., Sargent W.L.W., Barlow T.A., Churchill C.W., Vogt S.S., 1996, ApJS 107, 475
Meyer D.M., Lanzetta K.M., Wolfe A.M., 1995, ApJ 451, L13
Meyer D.M., Lauroesch J.T., 1999, ApJ 520, L103
Mo H.J., Miralda-Escudé J., 1996, ApJ 469, 589
Monier E.M., Turnshek D.A., Lupie O.L., 1998, ApJ 496, 177
Pei Y.C., Fall S.M., Bechtold J., 1991, ApJ 378, 6
Péquignot D., Aldrovandi S.M.V., 1986, A&A 161, 169
Petitjean P., Bergeron J., 1990, A&A 231, 309
Petitjean P., Bergeron J., Puget J.L., 1992, A&A 265, 375
Petitjean P., Rauch M., Carswell R.F., 1994, A&A 291, 29
Pettini M., Ellison S.L., Steidel C.C., Bowen D.V., 1999, ApJ 510, 576
Pettini M., Smith L.J., King D.L., Hunstead R.W., 1997, ApJ 486, 665
Prochaska J.X., Wolfe A.M., 1997, ApJ 474, 140
Prochaska J.X., Wolfe A.M., 1998, ApJ 507, 113
Prochaska J.X., Wolfe A.M., 2000, astro-ph/0002513
Rauch M., Sargent W.L.W., Barlow T.A., 1999, ApJ 515, 500
Savage B.D., Sembach K.R., 1996, ARAA 34, 279
Savaglio S., Panagia N., Stiavelli M., 1999, astro-ph/9912112
Seaton M.J., 1979, MNRAS 187,
Sembach K.R., Danks A.C., 1994, A&A 289, 539
Sembach K.R., Danks A.C., Savage B.D., 1993, A&AS 100, 107
Smette A., Robertson J.G., Shaver P.A., et al., 1995, A&AS 113, 199
Srianand R., Khare P.,1994, ApJ 428, 82
Srianand R., Kembhavi A., 1997, ApJ 478, 70
Srianand R., Petitjean P., 2000, A&A in press; astro-ph/0003301
Srianand R., Shankaranarayanan S., 1999, ApJ 518, 672
Steidel C.C., 1993, Shull J.M. & Thronson H.A., The Environment and Evolution of Galaxies, Proc. of the 3rd Teton Astronomy Conference, Dordrecht, Kluwer, p. 263
Stockes G.M., 1978, ApJS 36, 115
Thévenin F., 1998, Catalogue III/193, Bull. CDS, Vol. 49
Vidal-Madjar A., Andreani P., Cristiani S., et al., 1987, A&A 177, L17
Vladilo G., 1998, ApJ 493, 583
Vladilo G., Molaro P., Monai S., et al., 1993, A&A 274, 37
Vladilo G., Centurión M., Falomo R., Molaro P., 1997, A&A 327, 47
Welty D.E., Hobbs L.M., Kulkarny V.P., 1994, ApJ 436, 152
Welty D.E., Hobbs L.M., Lauroesch J.T., Morton D.C., Spitzer L., York D.G., 1999, ApJS 124, 465
Yun M.S., Ho P.T.P., Lo K.Y., 1994, Nature 372, 530
Zheng W., Kriss G.A., Telfer R.C., et al., 1997, ApJ 475, 469